P10.20 ESTIMATION OF LOW-LEVEL ATMOSPHERIC REFRACTIVITY GRADIENT USING RADAR GROUND ECHO COVERAGE

Shinju Park* and Frédéric Fabry
McGill University, Montreal, Quebec, Canada

1. INTRODUCTION

Radar beam propagation conditions are controlled by variation of refractive index of air *n* (or refractivity $N=(n-1)\times10^{-6}$) in the vertical. For example, if *N* decreases with height (*h*) due to the variation of pressure, temperature, and water vapor, the radar rays passing through layers of different *N* will bend downward. Based on the ray curvature compared with the curvature of the Earth (~ -157 km^{-1}), propagation conditions (*dN/dh)* are often categorized as i) ducting (*dN/dh*<-157 km^{-1}), ii) super-refraction (-157 km^{-1}<*dN/dh*<-79 km^{-1}), iii) normal refraction (-79 km^{-1}<*dN/dh*<0 km^{-1}), and iv) sub-refraction (*dN/dh*>0 km^{-1}) (e.g., Steiner and Smith 2002). In scanning radar observations, propagation conditions can affect particularly

- The determination of beam heights to locate weather/ground echoes (Bech et al. 2003),
- The detection of echoes for QPE (quantitative precipitation estimations) and QPF (quantitative precipitation forecasting) (e.g., Berenguer et al. 2006), and
- The quality of radar refractivity retrieval as discussed in Park and Fabry (2009).

Despite the importance of the knowledge on proper propagation conditions for radar data quality control, very few instruments measure the vertical gradient of refractivity. Radiosonde soundings can be useful, but its availability is low in terms of temporal and spatial (in the horizontal) resolution compared with those of radar observation.

Observing radar ground echo coverage, we know where ground echoes are. Also, we know the change of this coverage can be affected by *dN/dh*. Therefore, this study aims to investigate a method of extracting propagation conditions out of the radar observation of ground targets and to evaluate it.

**Corresponding author address:* Shinju Park, McGill Univ., Dept. of Atmospheric and Oceanic Sciences, Montreal, QC, CANADA, H3A2K6;
e-mail:shinju@meteo.mcgill.ca

2. METHOD

2.1 Data

Radar ground echo intensity and soundings have been collected over the domain of the S-Pol radar during the IHOP_2002 field experiment held in Oklahoma (Weckwerth et al. 2004). Fig. 1a shows the map of topography near the radar generated from the National Elevation Dataset of U.S Geological Survey (with a resolution of 1 arc-second). To enhance the contribution of echoes coming from ground targets, we use *NIQ* (Norm of In-phase and Quadrature), a measure of echo strength as following:

$$NIQ_i = 10\log_{10}\left(\left|X_i\right|\right), \text{ in dB,} \qquad [1]$$

where $X_i = \sum_{k=1}^{M} x_{i,k}$ for M samples of the complex $x_{i,k}$ (I, Q) at the *i*-th range gate. Two examples of *NIQ* fields at 0º elevation angle are shown in Fig. 1b and 1c observed on June 14, 2002 with no precipitation within the coverage. The large coverage of echo in Fig. 1b is possibly due to nocturnal radiative cooling. At other time, less coverage may result from sub-refraction conditions caused by surface heating (Fig. 1c).

According to Bean and Dutton (1968), *N* can be computed from pressure [*P* in hPa], temperature [*T* in Kelvin] and vapor pressure [*e* in hPa] as

$$N = 77.6\frac{P}{T} + 373000\frac{e}{T^2} \ . \qquad [2]$$

Then, it is the derivative of *N* with height that determines propagation conditions. Fig. 1d presents available *dN/dh* estimation from ISS (Integrated Sounding System seen in Fig. 1a) corresponding to the time of each radar scan on Fig. 1b and 1c. As we can see, the larger ground echo coverage corresponds to the larger negative values of *dN/dh*. In fact, we can

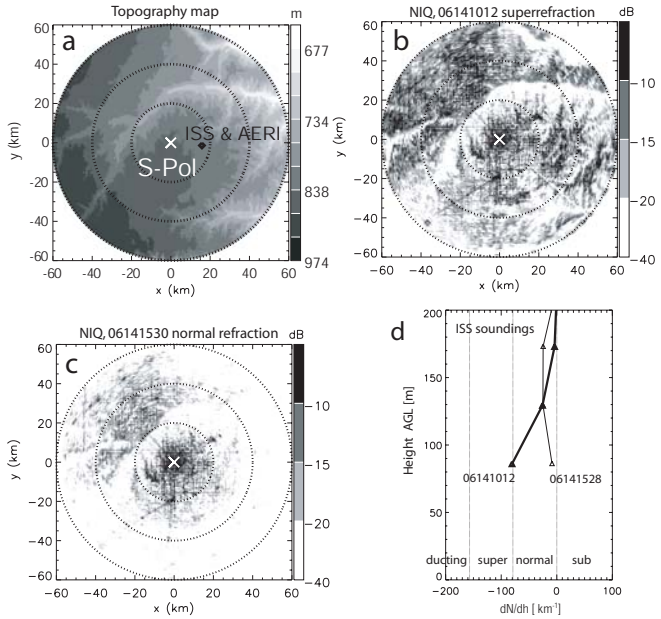

Fig.1: (a) Topography map within a range of 60 km. *NIQ* fields measured in (b) super-refractive, and (c) sub-refractive conditions. d) ISS soundings corresponding to the cases of (b) and (c).

simulate the expected ground echo coverage for a given *dN/dh* by computing the lowest ray height ($h(r)$) by ray tracing (Doviak and Zrnić 1993),

$$h(r) = \sqrt{r^2 + (R_e)^2 + 2rR_e \sin\theta} - R_e + H_r, \quad [3]$$

$$R_e = \frac{(R + H_r)}{1 + (R + H_r)\left(\frac{dn}{dh}\right)}.$$

where r is radar measurable range, θ is the elevation angle, H_r is the S-Pol radar height. The equivalent Earth radius (R_e) is obtained from the Earth radius (R) and the vertical gradient of refractive index. Subtracting the lowest ray heights from terrain heights (Fig. 2a), we can obtain ground target height (H_t) detectable by the radar. This can inform where the radar ray intercepts ground targets (e.g., the black areas shown in Fig. 2b and 2c) as a function of *dN/dh*.

2.2 Radar estimation of dN/dh

As we have shown, the *NIQ* field clearly shows changes in ground echo coverage. In parallel, we can simulate the ground targets intercepted by lowest ray heights. Hence, our method of estimating *dN/dh* is based on a best match between the simulation and the observation of the ground echo coverage. This is done by means of the following cost-function:

$$J\left(\frac{dN}{dh}\right) = \sum_{\Delta H_t} num_{\Delta H_t}\left[\frac{f_{obs}}{num_{\Delta H_t}} - f_{sim}\left(\frac{dN}{dh}\right)\right]^2. \quad [4]$$

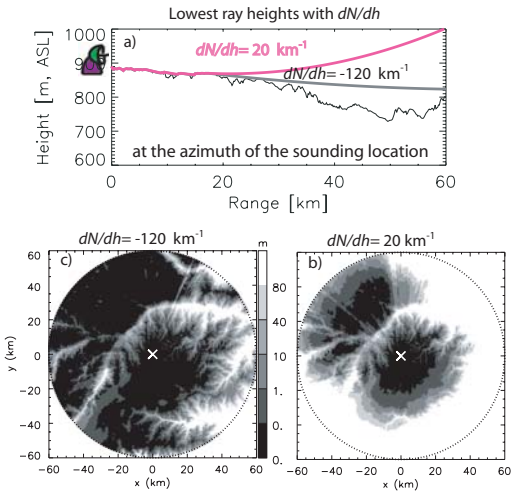

Fig.2: a) Illustration of the lowest ray height along the range for different *dN/dh*. A map of detectable ground target heights (H_t) for (b) a super-refraction or (c) a sub-refraction.

Since both observation and simulation have different variables to determine the ground coverage, we have parameterized them as probability functions f_{obs} and f_{sim} to be comparable to each other. First, Fig. 3a shows f_{obs} formulated with *NIQ* as

$$f_{obs} = \frac{10^{\frac{NIQ}{m}}}{10^{\frac{NIQ}{m}} + k\left(10^{\frac{NIQ\_thresh}{m}}\right)}, \qquad [5]$$

where *NIQ_thresh* is -20 dB, and *m* and *k* are weighting factors that assign values for detectable ground from 0 (no-ground) to 1 (ground).

Secondly, because simulated ground target heights are only a function of *dN/dh*, f_{sim} requires a reference height distribution of ground targets in the region that can be used to obtain ground coverage between 0 and 1. Such target height distribution should be independent of *dN/dh*. So, we have first selected periods of stable normal conditions of *dN/dh* observed by tethered sonde soundings (see section 3.2). For each *dN/dh* condition, a ground target height map can be generated as seen in Fig. 2. Then, the number ($num_{\Delta Ht}$ in [4]) of radar bins (e.g., 150 m in range and 1° in azimuth) with ΔH_t (e.g., 1 m, the height increment in the ground target heights) can be counted. By computing the ratio of the total values of f_{obs} with ΔH_t to this $num_{\Delta Ht}$, we can obtain an empirical cumulative probability of ground targets as a function of ground heights (black in Fig. 3b). Finally, f_{sim} is obtained by fitting (the grey) the mean of above probabilities.

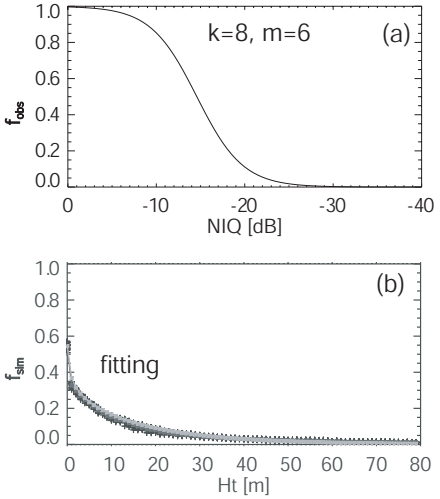

Fig. 3: Parameterization in the cost function: a) f_{obs} from the observation of *NIQ*, and b) f_{sim} from simulation of ground target heights.

3. VALIDATION CHALLENGES

For the entire period of experiments (about 45 days from May 11 to June 26 2002), radar ground echo coverage has been obtained in Fig. 4a using a threshold on *NIQ* of -20 dB. This threshold enables us to reject most precipitation echoes but does not fully guarantee to filter all. The frequency of observing enlarged ground echo coverage during the entire experimental period is relatively low (less than 0.1 seen in Fig. 4b).

In reality, sounding estimates of *dN/dh* from observations are limited in time and space and often uncertain near ground. Since the true low level *dN/dh* is not clearly known from both radar and sounding observations, we investigate a few validation approach based on available measurements.

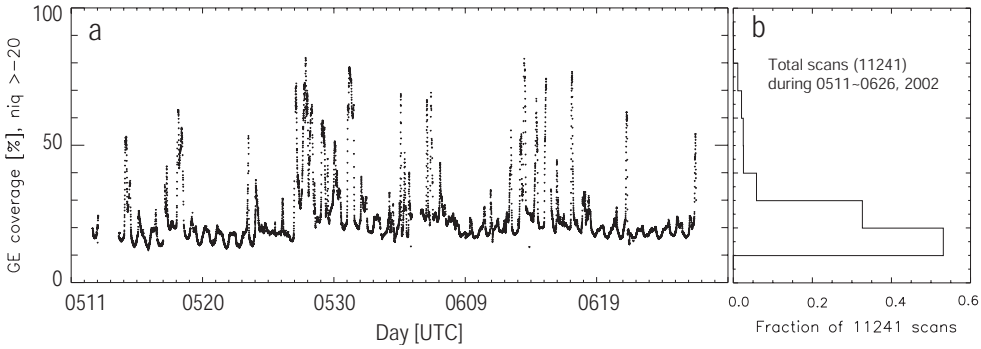

Fig. 4: a) Time series of ground echo coverage with *NIQ* larger than -20 dB within 60 km range in %. b) Histogram of ground echo coverage shown in a) over the total number of radar observation.

3.1 Sounding estimations of dN/dh

To compensate the lack of temporal resolution of radiosonde soundings, we have attempted to use the AERI (Atmospheric Emitted Radiance Interferometer) retrieved soundings sampled at 10 min resolution or better (Feltz et al. 2003). Conveniently, the AERI was located at the same site as ISS (Fig. 1a) and avoided precipitating periods. The AERI soundings are recorded at discrete heights (e.g., approximately at 43, 87, 131, and 175 m AGL at this location). We have interpolated these at the level of 80 m and smoothed them within 30 minutes. To be compared with the radar coverage seen in Fig. 4a, AERI soundings have been selected at closest time (within +/- 2.5 min difference) to the radar scan and plotted in Fig. 5. The dots (bars) represent the average (standard deviation) values of *dN/dh* within the interval of 10 % in the radar coverage. The lines represent expected (computed) ground coverage as a function of d*N/dh* for different ground target heights being less than 0, 5, 10, and 15 (m AGL). Smaller coverage corresponds well to the sub-refraction. As the coverage becomes larger, *dN/dh* decreases more, but not as much as the expected estimation because of either the small sampling number for super-refraction, ducting or some uncertainty in the observation from AERI as well as radar ground echo (e.g., overlapped with precipitation). Note that the proposed radar estimation is representative for the entire domain whereas the sounding estimates are often for instantaneous points. The may create some discrepancy on the comparison. Hence, the following section considers representativeness of *dN/dh* estimated from soundings.

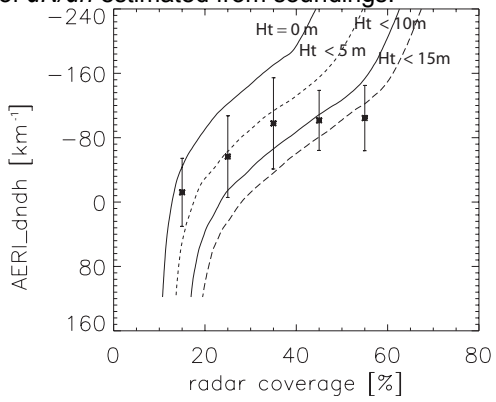

Fig. 5: Comparison between radar ground coverage and the estimated *dN/dh* from AERI sounding observation during 45 days.

3.2 Uncertainty of dN/dh from soundings

We have used tethered sonde soundings to access the representativeness uncertainty of *dN/dh* from soundings. Since this provides vertical profiles of atmospheric variables every second at certain heights (See Fig. 6a), we can estimate dN/dh fluctuation in time to be approximately converted into spatial variability. For example, for the normal conditions on June 14 seen in Fig.1c and 1d, the expected spread can be ± 20~30 km^{-1} (Fig. 6d). Although this value is mostly meaningful for a certain time period, it gives us a rough estimate of possible error values on sounding estimates of *dN/dh*.

3.3 Expected dN/dh for mixed air

When the measurement is not available or uncertain, we can also compute the expected *dN/dh* by differentiating each term in [2] with respect to height. If we assume a well mixed boundary layer (often the case on windy afternoon), the lapse rate of vapor pressure is expected to be small. Hence, for a given pressure, temperature, vapor pressure, and temperature lapse rate, we can compute dN/dh as a function of de/dh as shown in Fig. 7.

4. SELECTED RESULTS AND DISCUSSION

After minimizing [4] for entire experiment, we choose a dry period in mid May to present the results compared with AERI sounding. Since radar observation is performed near ground (~ 200 m AGL), the AERI *dN/dh* is also presented up to 200 m AGL. As we can see in Fig. 8, the radar (black) and AERI soundings (colors) show an excellent agreement. Especially diurnal cycles are well captured by both measurements. However, we also notice that local precipitation (that did not affect AERI) can still affect the radar estimation (e.g., in the morning on May 18). In addition, AERI observations are suspicious particularly in the afternoon with sudden decrease of dew-point temperature that creates the peak of sub-refraction (e.g., in the afternoon on May 22). It is possible that AERI may show a systematic bias because of its complicated retrieval algorithm based on observation as well as model profiles. In such cases, the analytical estimation from section 3.3 can also help us to understand if this high peak of *dN/dh* would be realistic or not. Otherwise, for super refraction

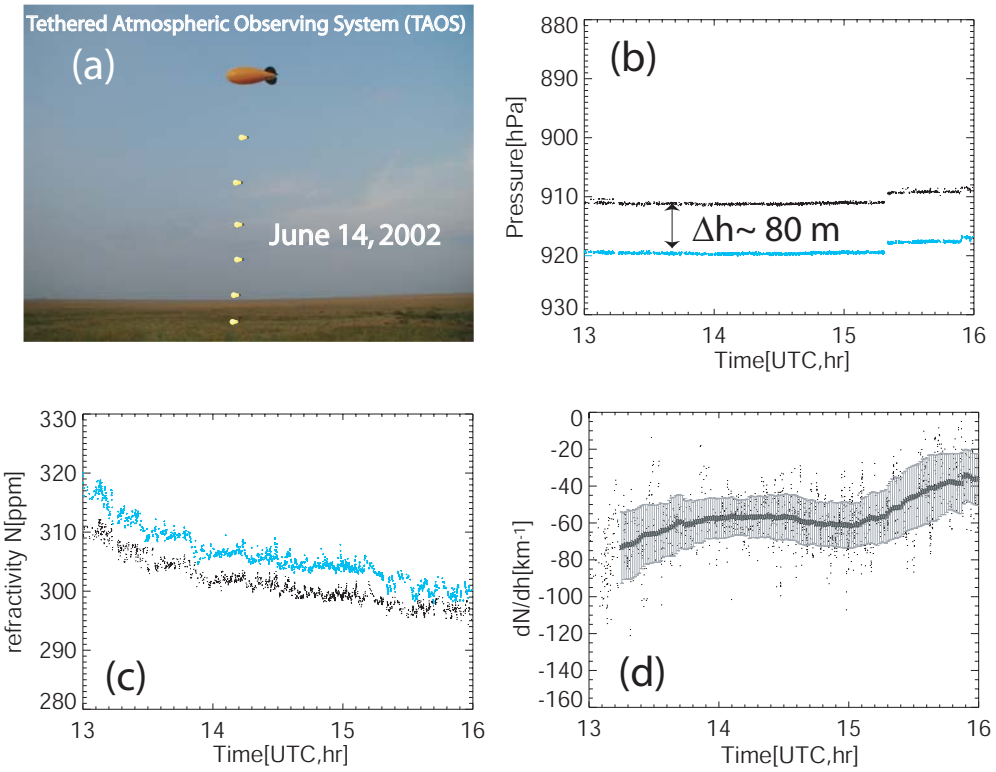

Fig. 6: An example of the tethered sonde soundings on June 14 during IHOP_2002. a) TAOS. Time series of pressure (b) and Refractivity estimates (c) at selected levels. d) The *dN/dh* computed. Estimates (dots) are averaged in 30 min (black line). The grey bars represent the values of standard deviation.

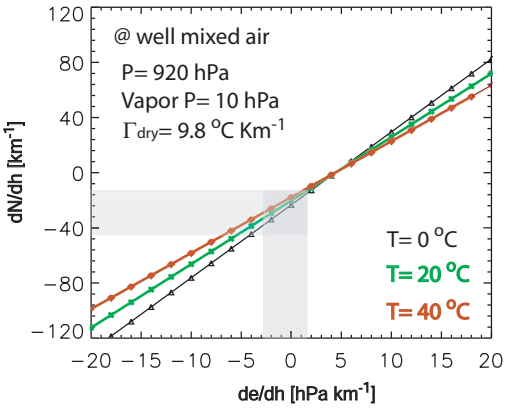

Fig. 7: An example of the expected *dN/dh* for given conditions. The grey shaded can be expected as values of reasonable *dN/dh*; i.e., around 0~-40 km^{-1}

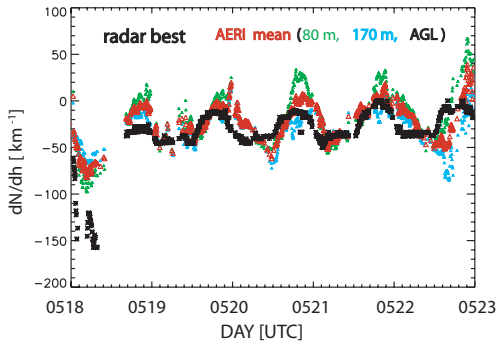

Fig. 8: dN/dh comparison between radar estimations and AERI observations.

conditions (normally before sunrise), our method has produced several promising estimations near ground (around 80 m AGL). For example, Fig. 9 shows the comparison between ISS and our estimate for the case seen in Fig. 1b.

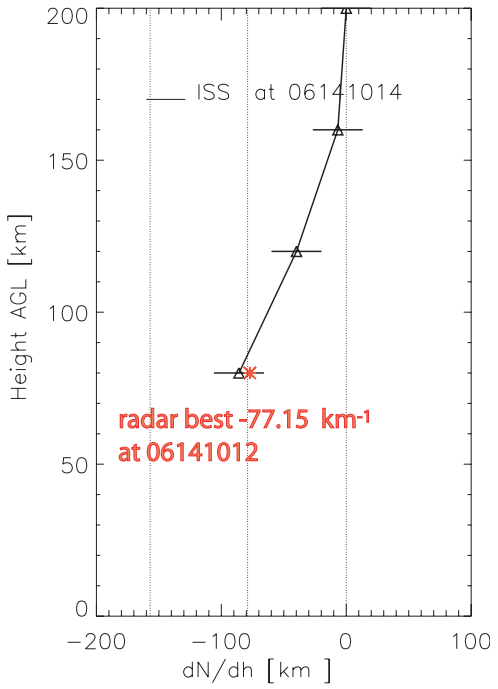

Fig. 9: dN/dh comparison between radar estimation and ISS observation on June 14 seen in Fig. 1. The error bars in the profile are based on the result of section 3.2.

5. CONCLUSIONS

Propagation conditions (*dN/dh*) play an important role in quality control of scanning radar observations. Since the ground echo coverage changes associated with *dN/dh* can be simulated, this study has attempted to estimate *dN/dh* from observed radar coverage. With the data collected from IHOP_2002, this simple and quick method has shown some skill in capturing the propagation conditions similar to these estimated from soundings. However, the evaluation of the method has been challenging because of 1) the lack of the conventional soundings in time and space, 2) the ambiguity in the separation of ground from weather echoes.

REFERENCES

Bean, B. R, and E. J. Dutton, 1968: *Radio Meteorology. National Bureau of Standards Monogr.*, No.92, National Bureau of Standards, 435 pp.

Bech, J., Codina, B., Lorente, J., Bebbington, D.: The sensitivity of single polarization weather radar beam blockage correction to variability in the vertical refractivity gradient, J. Atmos. And Oceanic Technol., 20, 845–855, 2003.

Berenguer, M., D. Sempere-Torres, C. Corral, and R. Sánchez-Diezma, 2006: A fuzzy logic technique for identifying non-precipitating echoes in radar scans. *J. Atmos. Oceanic Technol.,* 23, 1157–1180.

Doviak, R.J. and D.S. Zrnić, 1993: *Doppler Radar and Weather Observations.* 2nd Edition, Academy Press, Inc, pp 562.

Feltz, F., W.L. Smith, H.B. Howell, R.O. Knuteson, H. Woolf, and H.E. Revercomb, 2003: Near-continuous profiling of temperature, moisture, and atmospheric stability using the Atmospheric Emitted Radiance Interferometer (AERI). *J. Applied Meteor.*, 42, 584-597.

Park, S and F. Fabry, 2009: Simulation and Interpretation of the phase data used by radar refractivity retrieval algorithm. submitted to *J. Atmos. Ocean Technol.*,

Steiner, M. and J.A. Smith, 2002: Use of three-dimensional reflectivity structure for automated detection and removal of nonprecipitating echoes in radar data. *J. Atmos. Ocean Technol.*, 19, 673-686.

Weckwerth, T. M., D. B. Parsons, S. E. Koch, J. A. Moore, M. A. LeMone, B. B. Demoz, C. Flamant, B. Geerts, J. H. Wang, and W. F. Feltz, 2004: An overview of the International H2O Project (IHOP_2002) and some preliminary highlights. *Bull. Amer. Meteor. Soc.*, 85, 253-277.